bioRxiv preprint doi: https://doi.org/10.1101/627208; this version posted May 4, 2019. The copyright holder for this preprint (which was not certified by peer review) is the author/funder. All rights reserved. No reuse allowed without permission.

Flow-induced symmetry breaking in growing bacterial biofilms

Philip Pearce,[1] Boya Song,[1] Dominic J. Skinner,[1] Rachel Mok,[1,2] Raimo Hartmann,[3] Praveen K. Singh,[3] Jeffrey S. Oishi,[1,4] Knut Drescher,[3,5] and Jörn Dunkel[1]

[1] *Department of Mathematics, Massachusetts Institute of Technology, Cambridge MA 02139-4307, USA*
[2] *Department of Mechanical Engineering, Massachusetts Institute of Technology, Cambridge, MA 02139-4307, USA*
[3] *Max Planck Institute for Terrestrial Microbiology, Marburg, Germany*
[4] *Department of Physics, Bates College, Lewiston, ME 04240, USA*
[5] *Department of Physics, Philipps-Universität Marburg, Marburg, Germany*

(Dated: May 3, 2019)

Abstract. Bacterial biofilms are matrix-bound multicellular communities. Biofilms represent a major form of microbial life on Earth and serve as a model active nematic system, in which activity results from growth of the rod-shaped bacterial cells. In their natural environments, from human organs to industrial pipelines, biofilms have evolved to grow robustly under significant fluid shear. Despite intense practical and theoretical interest, it is unclear how strong fluid flow alters the local and global architectures of biofilms. Here, we combine highly time-resolved single-cell live imaging with 3D multi-scale modeling to investigate the effects of flow on the dynamics of all individual cells in growing biofilms. Our experiments and cell-based simulations reveal that, in the initial stages of development, the flow induces a downstream gradient in cell orientation, causing asymmetrical droplet-like biofilm shapes. In the later stages, when the majority of cells are sheltered from the flow by the surrounding extracellular matrix, buckling-induced cell verticalization in the biofilm core restores radially symmetric biofilm growth, in agreement with predictions from a 3D continuum model.

INTRODUCTION

Fluid flow is a key element of many natural and industrial environments in which bacteria form biofilms, from rivers [1], pipes [2] and filtration devices [3] to the human heart [4], intestines [5] and mouth [6], where biofilms cause a major economic and health burden. Hydrodynamic effects have been found to play a crucial role during the initial attachment of cells to surfaces [7]. Later in development, flow provides nutrients to surface-attached biofilm communities, removes metabolic waste products and affects quorum sensing molecules [8–10]. There is therefore intense practical and theoretical interest in understanding the interaction between biofilms and external flow fields [8, 11]. Identifying the multi-scale dynamics of such growth-active nematics under the influence of shear will be helpful when adapting current theories for active matter [12, 13] to describe and predict bacterial biofilm growth across model systems and species [14, 15]. Imposed fluid shear has been observed to produce striking aerofoil-like shapes [16–18] during the early stages of biofilm growth and, in some cases, long filaments or streamers that extend far downstream [1, 19]. It has often been assumed that the key driver of the observed architecture of biofilms in flow is bulk deformation or erosion of biofilm biomass [16, 19, 20]. Using single-cell live imaging [21, 22], we recently observed that cells within biofilms in high shear tend to align with the direction of fluid flow [17]. However, despite the extensive environmental relevance of flow-biofilm interactions, it has been unclear to what extent flow-induced cellular reorientations contribute to overall microscopic biofilm structure and macroscopic biofilm shape.

Here, we investigate comprehensively the effects of fluid shear on individual cell dynamics within growing *Vibrio cholerae* biofilms in 3D, by combining multi-scale modeling with highly time-resolved imaging at single-cell resolution. First, we establish the translational and orientational dynamics of cells within early-stage biofilm microcolonies in flow, by constraining an individual cell-based model with the imaging data. Subsequently, these dynamics are included in a minimal continuum model that identifies the physical processes necessary to explain the biofilm architectural development observed at the later stages. We find that the bulk biofilm dynamics are determined almost entirely by cellular orientations inside the biofilm, representing the local flow-induced nematic director field, rather than by deformation or cell erosion as has been previously hypothesized.

RESULTS

To investigate the effects of flow on biofilms in a broadly applicable setting, we imaged biofilm development on glass surfaces at cellular resolution in a flow channel with a shear rate of 2000 s^{-1} (Re $\approx$ 1), which is a typical order of magnitude for flows in natural and man-made environments containing bacteria [23–25]. To achieve the required time resolution, we improved a recently developed single-cell live-imaging technique, whereby adaptive confocal microscopy is combined with ground-truth-calibrated 3D image segmentation suitable for our model organism: *V. cholerae* with a straight cell shape ($\Delta crvA$), constitutively expressing a green fluorescent protein (sfGFP) (Fig. 1a,b). The increased time

bioRxiv preprint doi: https://doi.org/10.1101/627208; this version posted May 4, 2019. The copyright holder for this preprint (which was not certified by peer review) is the author/funder. All rights reserved. No reuse allowed without permission.

resolution, now at $\Delta t = 6$ min, enabled us to visualize previously inaccessible transient cell reorientations by the flow (Fig. 1a,b), in addition to reconstructing cell lineages and measuring cellular growth rates. By combining these new data with previously obtained data for larger biofilms [17], we obtained a comprehensive dataset showing the effects of fluid flow in unprecedented detail on biofilms growing from a single founder cell up to more than 2000 cells.

To understand the mechanical processes determining the shape and architecture of biofilms in flow, we developed a 3D multi-scale theoretical framework consisting of two separate models: a cell-based model and a continuum model. In the cell-based model, cells are represented as growing, dividing ellipsoids with pairwise interactions (Supplemental Material); parameters of this model were determined from single-cell biofilm experiments [17]. Movement of cells occurs through growth, cellular interactions mediated by extracellular matrix and adhesion proteins, and interactions with the flow, but no active motility exists inside *V. cholerae* biofilms. In our experiments, parent and daughter cells were observed to adhere after division for approximately one division time (Fig. 1a). We extended the cell-based model to account for this effect, using Hookean springs connected between the polar endpoints of parent and daughter cells, which persist for 90% of a division time (Supplemental Material). Furthermore, the model includes the effect that as the biofilm grows larger, it deforms the flow in a manner consistent with an approximately hemispherical object (Supplemental Material).

In the complementary continuum model, movement and alignment of biofilm matter is represented through a local mean velocity field $\boldsymbol{v}(t, \boldsymbol{x})$ and nematic 'Q-tensor' $\boldsymbol{Q} = S(\boldsymbol{nn} - \mathbf{1}/3)$ [12, 13, 26], where $S(t, \boldsymbol{x})$ is the nematic order parameter and $\boldsymbol{n}(t, \boldsymbol{x})$ is the nematic director field of cellular orientations. Within the biofilm, a modified incompressibility condition, $\nabla \cdot \boldsymbol{v} = g$, enforces constant growth with rate g; the assumption of a uniform growth rate g is valid as long as all cells have access to sufficient nutrients, which holds for the experimental conditions considered here (Supplemental Material). The effect of this growth, which is directed nematically because cells elongate and divide along their longest axis [27], is imposed by including an additional active term in the stress [28]. Over growth timescales, the passive part of the constitutive relationship can be approximated as purely viscous with effective viscosity μ, yielding a stress tensor $\boldsymbol{\sigma} = -p\mathbf{1} + \mu(\nabla \boldsymbol{v} + \nabla \boldsymbol{v}^T) - 2\mu g \boldsymbol{Q}$ in total (Supplemental Material), where p is the pressure. This constitutive law was simulated in the open-source solver Dedalus [29], using a phase-field variable to track the expansion of the biofilm [30, 31]; the nematic order field was imposed to be qualitatively similar to experimental data (Supplemental Material). Using this model, we could assess the effect of various observed cell align-

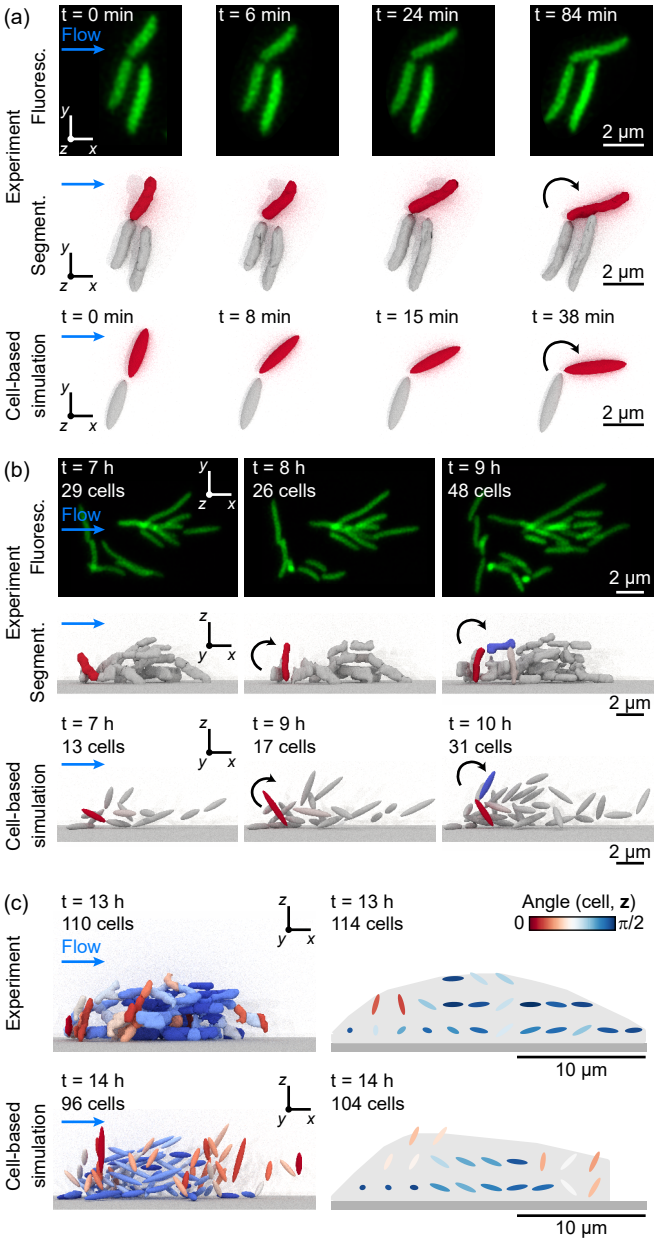

FIG. 1. Mechanisms for flow-induced cell orientation dynamics in the initial phase of biofilm growth. (a) Cells in direct contact with the surface align with the flow as a result of a torque generated by a combination of the fluid drag and asymmetrical attachment to their parent cell at the pole. Fluorescence images show projection of a confocal z-stack. (b) Cells at the front of the biofilm (red) align vertically as a result of the torques τ_{drag} and τ_{shear}. When a vertically-oriented cell (red) divides, the daughter cell (blue), if exposed to shear, aligns with the flow. (c) In the early stages of growth, cells are predominantly aligned with the flow, with some vertical cells on the upstream side of the biofilm. The right-hand panels show averaged nematic alignment fields for several experiments ($n = 3$, top) and simulations ($n = 10$, bottom) along the midplane of the biofilm. In each case, the grey area denotes the region inside the convex hull around gridpoints with a cell number density higher than 0.05 μm^{-3} per biofilm.

bioRxiv preprint doi: https://doi.org/10.1101/627208; this version posted May 4, 2019. The copyright holder for this preprint (which was not certified by peer review) is the author/funder. All rights reserved. No reuse allowed without permission.

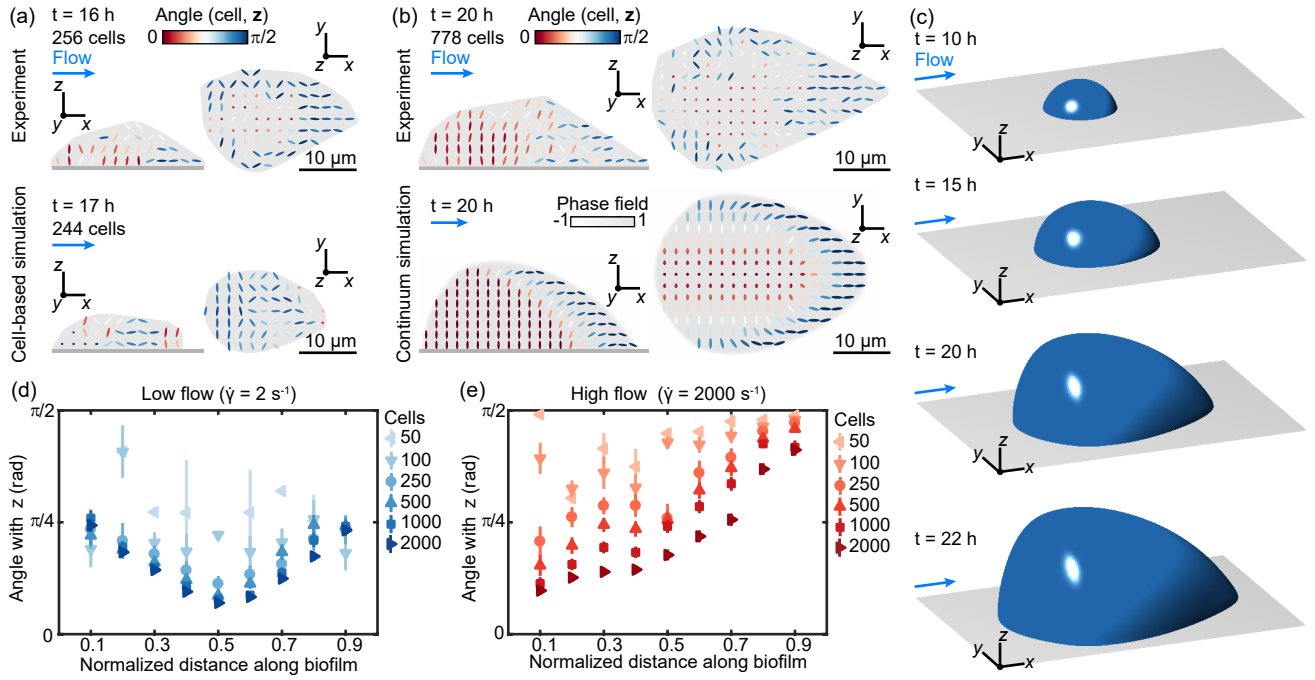

FIG. 2. A wave of cell verticalization travels downstream through the biofilm in the second phase of biofilm growth. (a) At the beginning of this phase, a small group of cells is verticalized at the front of the biofilm by a combination of cell-cell interactions and fluid shear. (b) The fraction of vertical cells increases as the biofilm grows. The downstream region of flow-aligned cells leads to distinctive droplet-like shapes that are captured in (a) cell-based and (b) continuum simulations. For the experiments ($n = 3$) and cell-based simulations ($n = 10$), the grey area denotes the region inside the convex hull around gridpoints with a cell number density higher than 0.1 μm^{-3} per biofilm. (c) 3D renderings of shapes generated by the continuum simulations. The isosurface $\phi = 0$ of the phase-field variable ϕ is shown (Supplemental Material). (d) In low flow environments, a central core of the biofilm is verticalized owing to a buckling instability induced by growth and surface attachment. (e) Strong flow causes symmetry breaking and a growing group of vertically aligned cells at the front of the biofilm. Error bars show the standard error for gridpoints spaced 2 μm throughout $n = 3$ biofilms in each case.

ment fields $\boldsymbol{n}(t, \boldsymbol{x})$ on biofilm growth and shape.

The combined multi-scale models and experiments revealed that the full growth and cellular alignment program of bacterial biofilms in flow can be categorized into three distinct physical regimes.

During the initial biofilm growth regime (Fig. 1), the majority of cells are exposed to the flow. The presence of strong shear breaks the otherwise hemispherically-symmetric colony growth, and two key physical processes dominate the cell alignment dynamics. First, daughter cells are reoriented after division to align with the flow by a drag-induced torque caused by the combination of the flow and the polar adhesion to their parent cell (Fig. 1a). Specifically, a horizontal ellipsoidal cell of length l and width r constrained at one pole, with its longest axis perpendicular to a flow of speed U, is expected to feel a torque $\tau_{\text{drag}} \sim Dl$, where D is the drag $D \sim G_1 \mu l U$; here G_1 is a geometric factor [32]. Thus, using $\boldsymbol{v} = \dot{\gamma} z \hat{\mathbf{x}}$, we have $\tau_{\text{drag}} \sim G_1 \mu l^2 h \dot{\gamma}$, where h is the height of the cell centroid from the surface. Second, cells experience a separate shear-induced torque, which causes a cell's longest axis to rotate about the axis perpendicular to the plane of the flow [33]. For a horizontal cell whose longest axis is parallel to the flow, this torque is approximately $\tau_{\text{shear}} \sim G_2 \mu l r^2 \dot{\gamma}$; here G_2 is a second geometric factor [34]. Both torques are expected to be of the same order of magnitude $\tau \sim 1$ pNμm, which is not strong enough to rip fully surface-attached cells from the floor [35]. However, the flow-induced torques act together to cause the verticalization of daughter cells at the front of the biofilm that are not fully surface-attached [36, 37], or that have been partially verticalized by a peeling instability induced by nearby cells [35] (Fig. 1b). Both flow-induced cell reorientation processes were captured by the cell-based model (Fig. 1a,b). The simulations also recreated the cell alignment fields, consisting of mainly flow-aligned cells with some vertical cells at the front of the biofilm (Fig. 1c), suggesting that an applied shear is sufficient to explain their observation in our experiments.

In the second growth regime (Fig. 2), cells in the outer shell of the biofilm are still exposed to the flow, whereas the core of the biofilm is sheltered by surrounding cells and extracellular matrix. The location within the biofilm determines which cell alignment dynamics dominates: cells that are exposed to the flow at the upstream end

bioRxiv preprint doi: https://doi.org/10.1101/627208; this version posted May 4, 2019. The copyright holder for this preprint (which was not certified by peer review) is the author/funder. All rights reserved. No reuse allowed without permission.

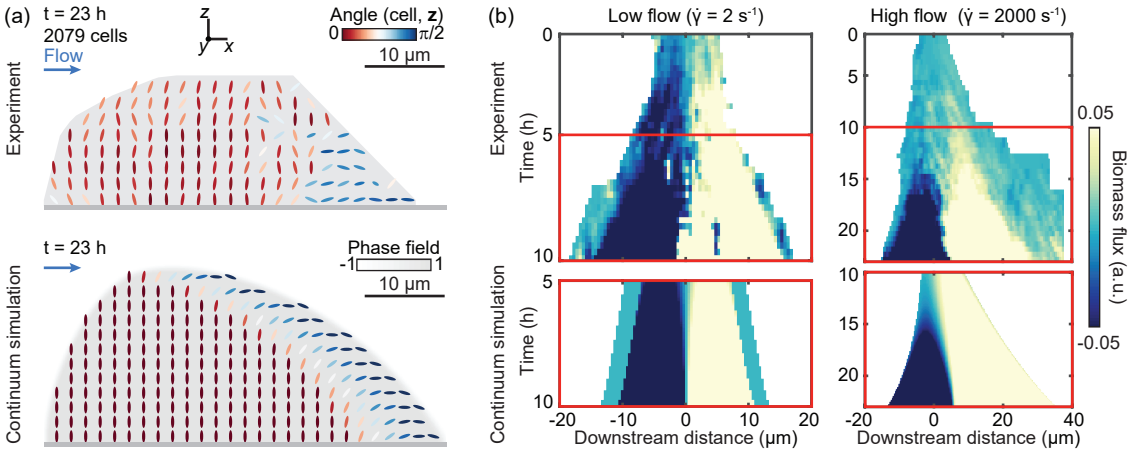

FIG. 3. Biofilms transition from asymmetric to symmetric growth in the final phase of their development in flow. (a) In the final phase of growth, most of the cells in the biofilm are vertical, with only a small region of flow-aligned cells on the downstream side. The grey area denotes the region inside the convex hull around gridpoints with a cell number density higher than 0.1 μm^{-3} per biofilm ($n = 3$). (b) Growth-induced cumulative biomass flux through the yz-plane at each downstream distance; positive and negative values correspond to flux in the downstream and upstream direction, respectively. In low flow, growth is always symmetric (left). In high flow (right), growth symmetry is broken in the early phases, but as more cells verticalize, the biofilm transitions to symmetric growth, which is also captured by continuum simulations (bottom). In experiments (top panels, $n = 3$), biomass flux measurements were obtained using optical flow [17]. In continuum simulations (bottom), the solution for the flow field inside the biofilm was used to calculate cumulative biomass flux.

of the biofilm continue to be realigned vertically owing to the torques τ_{drag} and τ_{shear} (Fig. 2a,b), whereas cells elsewhere in the outer shell of the biofilm continue to align with the flow, mainly owing to τ_{drag}, maintaining asymmetric growth of the biofilm overall. In particular, growth of the horizontally-aligned cells in the downstream region causes distinctive droplet-like shapes when viewed from above, which is captured by continuum simulations of growing biofilms with cell alignment fields consisting of a downstream region of flow-aligned cells (Fig. 2a-c). However, cells in the core of the biofilm are not exposed to the flow, so their dynamics are dominated by growth; they are subject to a growth-induced buckling instability [35, 38–40] and the "inverse domino" effect of being surrounded by already vertical cells [35]. The combination of the flow-induced and growth-induced realignment processes leads to a gradient in the vertical alignment of cells from the upstream end to the downstream end of the biofilm and a wave of cellular verticalization that travels through the biofilm from upstream to downstream (Fig. 2e).

In the third growth regime (Fig. 3), the majority of cells in the biofilm are sheltered from the flow, and growth dominates the cell alignment dynamics. Owing to the growth-induced buckling instability and verticalization wave, biofilms contain a core of highly vertically-aligned cells (Fig. 3a), consistent with the findings of several recent experimental studies of biofilm growth in no flow or very weak flow, where the shear is not strong enough to reorient cells [17, 19, 35]. We used the continuum model to investigate how the observed cell alignment fields in this phase determine biofilm growth and shape. In earlier stages of development, when cells tend to be aligned in a gradient from vertical in the upstream region to horizontal in the downstream region, growth is predominantly in the downstream direction (Fig. 3b). As the region of vertical cells expands downstream, growth becomes more symmetric, eventually resembling the symmetric radial expansion of biofilms in weak flow (Fig. 3b). The agreement between the growth dynamics observed in our experiments and continuum simulations suggests that the competition between flow-aligned and vertical growth is sufficient to explain biofilm growth in flow for biofilms with up to several thousand cells.

In the past, deformation and shear-induced erosion have been hypothesized to explain the flow-induced symmetry breaking of bacterial biofilms in flow [16, 19]. Although this is expected to be true for the extremely large shear rates experienced in turbulent flow, or for bacterial species with weak matrix, we discovered that deformation and erosion processes are unable to account for the architectures of biofilms in our experiments ($\dot{\gamma} = 2000\,\text{s}^{-1}$). In this physiologically relevant flow regime, shear-induced erosion is resisted by the increased production of cell-cell adhesion proteins [17]. Although some cells are still carried away by the flow (Fig. 1b), the effect of erosion is negligible for the architecture dynamics. Deformation is also negligible for biofilms in our experiments. The fluid, which has the viscosity of water μ_w, exerts a stress on the biofilm of approximate magnitude $\mu_w\dot{\gamma}$ so that, by matching stresses at the fluid-biofilm interface, the strain needed to balance the external stress is approximately

bioRxiv preprint doi: https://doi.org/10.1101/627208; this version posted May 4, 2019. The copyright holder for this preprint (which was not certified by peer review) is the author/funder. All rights reserved. No reuse allowed without permission.

$\epsilon = \mu_w \dot{\gamma}/G \sim 10^{-3}$, since biofilms have hydrogel-like material properties with elastic modulus $G \sim 10^3$ Pa [41]. Therefore a *V. cholerae* biofilm will not be significantly deformed by the flow, and over growth time scales, a balance between the internal elasticity and external flow appears instantaneous, with growth then occurring along nematic directions. This supports the hypothesis that nematically-aligned growth is the key determinant of bacterial biofilm shape.

CONCLUSION

The above experimental and numerical results show that flow initially breaks the symmetry in the cell alignment field of growing biofilms. Because cells grow in the direction of their longest axis, the altered cell orientations significantly affect biofilm architecture, causing distinctive droplet-like shapes. In later stages, cells verticalize in a wave that travels from the upstream end to the downstream end of the biofilm, causing a transition from asymmetric flow-aligned growth to symmetric growth of the biofilm colony, even in the presence of flow. In contrast with previous assumptions, deformation and shear-induced erosion are not important determinants of biofilm architecture for the shear rates studied here. Individual cell dynamics are a crucial component of the architecture of growing biofilms, and must be tracked carefully when characterizing the effect of external fields on biofilm systems.

Acknowledgments

The authors would like to thank Hannah Jeckel, Takuya Ohmura and Vili Heinonen for helpful discussions. Computations of the continuum model were performed on the *Leavitt* system at the Bates College High Performance Computing Center. This work was partially supported by an Edmund F. Kelly Research Award (J.D.) and James S. McDonnell Foundation Complex Systems Scholar Award (J.D.), as well as the Human Frontier Science Program (K.D., CDA00084/2015-C), the Max Planck Society (K.D.), the European Research Council (K.D., StG-716734), and the Deutsche Forschungsgemeinschaft (SFB 987).

[1] L. Hall-Stoodley, J. W. Costerton, and P. Stoodley, Nat. Rev. Microbiol. **2**, 95 (2004).
[2] T. Liu, Y. F. Cheng, M. Sharma, and G. Voordouw, J. Petrol. Sci. Eng. **156**, 451 (2017).
[3] D. R. Simpson, Water Res. **42**, 2839 (2008).
[4] K. Werdan, S. Dietz, B. Löffler, S. Niemann, H. Bushnaq, R.-E. Silber, G. Peters, and U. Mueller-Werdan, Nat. Rev. Cardiol. **11**, 35 (2014).
[5] C. M. Dejea, P. Fathi, J. M. Craig, A. Boleij, R. Taddese, A. L. Geis, X. Wu, C. E. D. Shields, E. M. Hechenbleikner, D. L. Huso, *et al.*, Science **359**, 592 (2018).
[6] P. E. Kolenbrander, Annu. Rev. Microbiol. **54**, 413 (2000).
[7] S. Lecuyer, R. Rusconi, Y. Shen, A. Forsyth, H. Vlamakis, R. Kolter, and H. A. Stone, Biophys. J. **100**, 341 (2011); A. S. Utada, R. R. Bennett, J. C. Fong, M. L. Gibiansky, F. H. Yildiz, R. Golestanian, and G. C. Wong, Nat. Commun. **5**, 4913 (2014); G. A. O'Toole and G. C. Wong, Curr. Opin. Microbiol. **30**, 139 (2016).
[8] P. S. Stewart, Biofouling **28**, 187 (2012).
[9] M. K. Kim, F. Ingremeau, A. Zhao, B. L. Bassler, and H. A. Stone, Nat. Microbiol. **1**, 15005 (2016).
[10] P. K. Singh, S. Bartalomej, R. Hartmann, H. Jeckel, L. Vidakovic, C. D. Nadell, and K. Drescher, Curr. Biol. **27**, 3359 (2017).
[11] Y. Yawata, J. Nguyen, R. Stocker, and R. Rusconi, J. Bacteriol. **198**, 2589 (2016).
[12] M. C. Marchetti, J. F. Joanny, S. Ramaswamy, T. B. Liverpool, J. Prost, M. Rao, and R. A. Simha, Rev. Mod. Phys. **85**, 1143 (2013).
[13] A. Doostmohammadi, J. Ignés-Mullol, J. M. Yeomans, and F. Sagués, Nat. Commun. **9**, 3246 (2018).
[14] R. J. Allen and B. Waclaw, Rep. Prog. Phys. **82**, 016601 (2018).
[15] A. Welker, T. Cronenberg, R. Zöllner, C. Meel, K. Siewering, N. Bender, M. Hennes, E. R. Oldewurtel, and B. Maier, Phys. Rev. Lett. **121**, 118102 (2018).
[16] B. Purevdorj, J. W. Costerton, and P. Stoodley, Appl. Environ. Microbiol. **68**, 4457 (2002).
[17] R. Hartmann, P. K. Singh, P. Pearce, R. Mok, B. Song, F. Díaz-Pascual, J. Dunkel, and K. Drescher, Nat. Phys. **15**, 251 (2019).
[18] I. Hug, S. Deshpande, K. S. Sprecher, T. Pfohl, and U. Jenal, Science **358**, 531 (2017).
[19] K. Drescher, Y. Shen, B. L. Bassler, and H. A. Stone, Proc. Natl. Acad. Sci. U.S.A. **110**, 4345 (2013).
[20] M. Klotz, M. Kretschmer, A. Goetz, S. Ezendam, O. Lieleg, and M. Opitz, RSC Adv. **9**, 11521 (2019).
[21] K. Drescher, J. Dunkel, C. D. Nadell, S. van Teeffelen, I. Grnja, N. S. Wingreen, H. A. Stone, and B. L. Bassler, Proc. Natl. Acad. Sci. U.S.A. **113**, E2066 (2016).
[22] J. Yan, A. G. Sharo, H. A. Stone, N. S. Wingreen, and B. L. Bassler, Proc. Natl. Acad. Sci. U.S.A. **113**, E5337 (2016).
[23] S. Samijo, J. Willigers, R. Barkhuysen, P. Kitslaar, R. Reneman, P. Brands, and A. Hoeks, Cardiovasc. Res. **39**, 515 (1998).
[24] A. Campesi, M. O. Cerri, C. O. Hokka, and A. C. Badino, Bioproc. Biosyst. Eng. **32**, 241 (2009).
[25] H. C. Fu, T. R. Powers, and R. Stocker, Proc. Natl. Acad. Sci. U.S.A. **109**, 4780 (2012).
[26] P.-G. De Gennes and J. Prost, *The Physics Of Liquid Crystals (International Series Of Monographs On Physics)* (Oxford University Press, 1995).
[27] F. Chang and K. C. Huang, BMC Biol. **12**, 54 (2014).
[28] Z. You, D. J. G. Pearce, A. Sengupta, and L. Giomi, Phys. Rev. X **8**, 031065 (2018).
[29] *Dedalus Project*, `http://dedalus-project.org`.

bioRxiv preprint doi: https://doi.org/10.1101/627208; this version posted May 4, 2019. The copyright holder for this preprint (which was not certified by peer review) is the author/funder. All rights reserved. No reuse allowed without permission.

[30] T. Zhang, N. G. Cogan, and Q. Wang, SIAM J. Appl. Math. **69**, 641 (2008).

[31] S. Srinivasan, N. C. Kaplan, and L. Mahadevan, eLife (2019, in press).

[32] J. Happel and H. Brenner, *Low Reynolds number hydrodynamics: with special applications to particulate media* (Kluwer, Dordrecht, 1983).

[33] G. B. Jeffery, Proc. Royal Soc. A **102**, 161 (1922).

[34] D. Saintillan and M. J. Shelley, in *Complex Fluids in Biological Systems* (Springer, 2015) pp. 319–355.

[35] F. Beroz, J. Yan, Y. Meir, B. Sabass, H. A. Stone, B. L. Bassler, and N. S. Wingreen, Nat. Phys. **14**, 945 (2018).

[36] B. J. Cooley, S. Dellos-Nolan, N. Dhamani, R. Todd, W. Waller, D. Wozniak, and V. D. Gordon, New J. Phys. **18**, 045019 (2016).

[37] M.-C. Duvernoy, T. Mora, M. Ardré, V. Croquette, D. Bensimon, C. Quilliet, J.-M. Ghigo, M. Balland, C. Beloin, S. Lecuyer, and N. Desprat, Nat. Commun. **9**, 1120 (2018).

[38] M. Asally, M. Kittisopikul, P. Rué, Y. Du, Z. Hu, T. Çağatay, A. B. Robinson, H. Lu, J. Garcia-Ojalvo, and G. M. Süel, Proc. Natl. Acad. Sci. U.S.A. **109**, 18891 (2012).

[39] M. A. Grant, B. Wacław, R. J. Allen, and P. Cicuta, J. Royal Soc. Interface **11**, 20140400 (2014).

[40] Z. You, D. J. Pearce, A. Sengupta, and L. Giomi, arXiv:1811.08875 (2018).

[41] J. Yan, A. Moreau, S. Khodaparast, A. Perazzo, J. Feng, C. Fei, S. Mao, S. Mukherjee, A. Košmrlj, N. S. Wingreen, B. L. Bassler, and H. A. Stone, Adv. Mater. **30**, 1804153 (2018).